

# Detecting Human Artifacts from Text-to-Image Models

Kaihong Wang\*  
Boston University  
kaiwkh@bu.edu

Lingzhi Zhang  
Adobe Research  
lingzrza@adobe.com

Jianming Zhang  
Adobe Research  
jianmzha@adobe.com

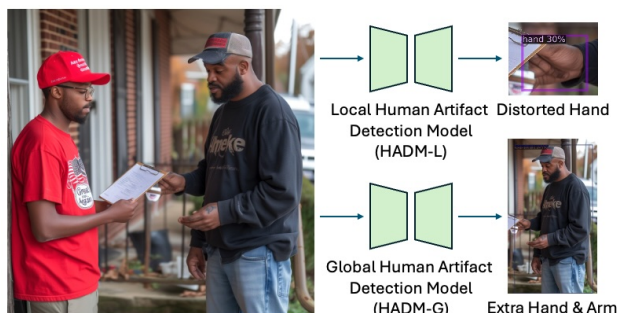
## Abstract

Despite recent advancements, text-to-image generation models often produce images containing artifacts, especially in human figures. These artifacts appear as poorly generated human bodies, including distorted, missing, or extra body parts, leading to visual inconsistencies with typical human anatomy and greatly impairing overall fidelity. In this study, we address this challenge by curating Human Artifact Dataset (HAD), the first large-scale dataset specifically designed to identify and localize human artifacts. HAD comprises over 37,000 images generated by several popular text-to-image models, annotated for human artifact localization. Using this dataset, we train the Human Artifact Detection Models (HADM), which can identify diverse artifact types across multiple generative domains and demonstrate strong generalization, even on images from unseen generators. Additionally, to further improve generators' perception of human structural coherence, we use the predictions from our HADM as feedback for diffusion model finetuning. Our experiments confirm a reduction in human artifacts in the resulting model. Furthermore, we showcase a novel application of our HADM in an iterative inpainting framework to correct human artifacts in arbitrary images directly, demonstrating its utility in improving image quality. Our dataset and detection models are available at: <https://github.com/wangkaihong/HADM>.

## 1. Introduction

Recent advancements in text-to-image generation [5, 26, 40, 50, 57, 64] have led to applications in various areas, including image editing [1, 13, 45], representation learning from synthetic data [6, 47, 51, 52], and more. Current state-of-the-art diffusion models [12, 15, 30, 31, 37, 40] are primarily trained on large proprietary datasets, with prohibitively high training costs, resulting in impressive overall quality improvements in generated images. Despite these advancements, **human artifacts** remain persistent challenges across

\*Work partially done during an internship at Adobe.



GPT-4o: The image **does not contain any noticeable human artifacts**. Both individuals appear to have the correct number of arms, legs, and feet with no distortions or missing parts. Therefore, I would classify the severity of the artifact as: 1: No human artifact. Both individuals are depicted naturally with no visual disturbances.

LLaVA-1.6: In the image provided, there are **no obvious artifacts** that would fit into the categories you've listed. The individuals appear to be in a normal state with **no visible distortions or missing body parts** that would classify as artifacts. The image seems to depict a typical human interaction with no significant anomalies that would be considered artifacts.

Figure 1. Comparison between our Human Artifact Detection Models (HADM) and state-of-the-art vision-language models in detecting human artifacts in an influential deepfake image circulating on social media during the 2024 U.S. presidential election. While advanced VL models fail to detect visible artifacts of the right human figure in the image (shown in the responses at the bottom), our models successfully identify and localize the distorted hands and the extra limb (top right). Source: <https://farid.berkeley.edu/deepfakes2024election/>.

models, frequently leading to anomalies such as distorted, missing, or extra body parts. Such issues significantly compromise **human structural coherence**, which we define as the consistency with typical human anatomy, and greatly undermine the overall fidelity of images. For instance, in Fig. 1, artifacts on the human figure on the right are clearly visible, as highlighted by detection results from our models. However, when analyzed by advanced vision-language (VL) models, such as GPT-4o [33] and LLaVA [23], these artifacts are not identified. This highlights the surprisingly limited grasp of human structural coherence even in state-of-the-art VL models, despite their strong performance in various downstream tasks. In this work, we propose an alternative approach that effectively detects and addresses hu-

man artifacts in images from various text-to-image models.

Existing works on evaluating the quality of images from generative models primarily focus on global attributes such as text-image alignment [11, 17, 22] and aesthetics [14, 20, 53–55], or general local artifacts [20, 61]. While there are theoretical correlations between these aspects and the detection of human artifacts, current approaches remain ineffective, often being diverted by irrelevant elements such as the overall layout of the images, non-human objects in the background, or other factors that disrupt the evaluation of human artifacts.

To effectively identify different types of human artifacts in generated images, we first define two primary categories: local artifacts, which focus on localized regions of human body parts with poorly rendered features (e.g., flawed patterns, textures, or shapes), and global artifacts, which reflect structural or anatomical inconsistency to typical human figures, such as missing or extra body parts. We curate the first dataset focusing on human artifacts in synthetically generated images, namely Human Artifact Dataset (HAD), from four widely used diffusion models, i.e., SDXL [37], DALLE-2 [30], DALLE-3 [31], and Midjourney [12], annotated with bounding boxes and artifact types, resulting in 37,554 samples with 84,852 labeled instances covering various types of local and global artifacts.

We train the Human Artifact Detection Models (HADM) on our dataset to identify local and global human artifacts, respectively. Utilizing a state-of-the-art architecture and regularized with diverse real human images, HADM demonstrate significant performance advantages over existing methods, including advanced VL models, excelling at detecting various human artifacts in our dataset and generalizing effectively to images from more advanced generators not included in the training data.

Furthermore, beyond identifying human artifacts, we demonstrate that HADM provide valuable guidance for mitigating these artifacts. Specifically, we finetune a diffusion model on images paired with special identifiers representing different types of detected human artifacts, which are later applied as negative prompts during inference. This approach enables the diffusion model to recognize and avoid poorly generated human features, resulting in reduced human artifacts, as validated by our experimental results. Additionally, we showcase another utility of HADM as a guide to effectively automate the inpainting pipeline to identify and rectify human artifacts in arbitrary images.

To summarize, the contributions of this work include:

- We curate the Human Artifact Dataset (HAD), the first dataset dedicated to detecting human artifacts in images generated by text-to-image models, featuring bounding box annotations for precise localization.
- By training on HAD, the Human Artifact Detection Models (HADM) effectively detect various human artifacts

from different generative models, demonstrating robust performance and generalization on images from previously unseen domains.

- We highlight the impactful application of HADM’s predictions as guidance for finetuning diffusion models and assisting inpainting workflows, further reducing human artifacts in generated images.

## 2. Related Works

### 2.1. Text-to-Image Generation

Text-to-image (T2I) models have evolved through several different main architectures. GANs [50, 57, 64] were early approaches, training a generator-discriminator pair to produce realistic images. Autoregressive models [26], such as DALLE [39], introduced sequential generation, later refined by VQ-VAE [5] for better control and detail. The current state-of-the-art, Diffusion Models (DMs) [9, 29, 48], generate images by reversing noise, capturing high diversity and quality. Latent Diffusion Models (LDMs) [40] improve efficiency by operating in latent space, with SDXL [37] enabling high-resolution synthesis.

### 2.2. Evaluation of Text-to-Image Generators

Typical evaluation metrics for text-to-image models include automated scores such as FID [8, 35], Inception Score [42], and CLIPScore [7]. However, with rapid advancements in T2I models, human perception evaluation [34, 63] has become increasingly important, and more recent works propose comprehensive benchmarks that assess various aspects of T2I generation [11, 16, 17, 22, 53]. Inspired by Reinforcement Learning from Human Feedback (RLHF), several recent works aim to model human preference, mainly on aesthetics or identifying general artifacts, from curated datasets and further align T2I models or directly address local artifacts. HPD-v1 [54] assigns scores to images to guide models toward human-preferred quality, while Pick-A-Pic [14] and ImageReward [55] use paired comparisons for more effective preference modeling. RichHF-18K [20] further includes annotations for general local artifacts, implausibilities, and misalignment between text and image. Zhang et al. [61] train binary segmentation model on their dataset with pixel-level annotations. Despite these efforts, none of these methods explicitly identify and localize human artifacts. Our proposed dataset, Human Artifact Dataset, provides bounding box annotations for various human artifacts, creating a solid foundation for effective human artifact detection and improvement.

### 2.3. Human Artifacts in Text-to-Image Generation

Hand generation issues are particularly prevalent in T2I models, with most of the research on human artifacts focusing on this specific challenge. HandRefiner [25] and

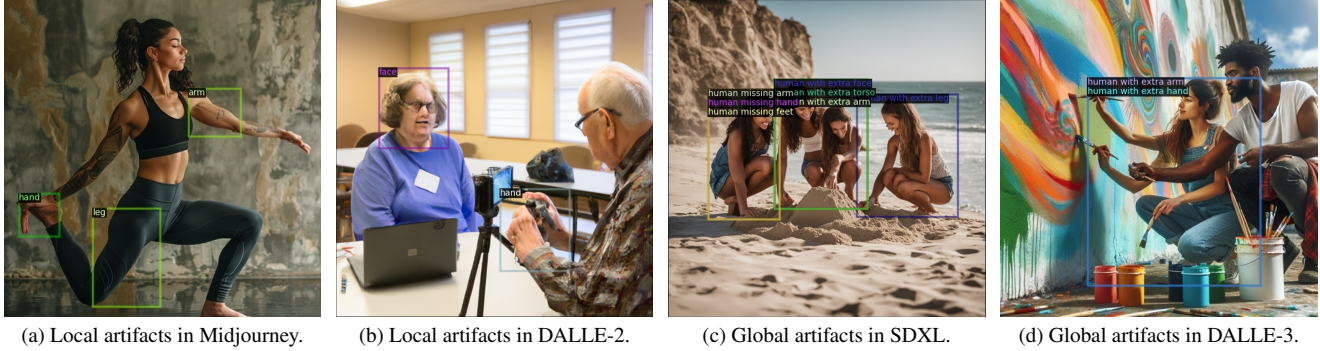


Figure 2. Example annotations from different generators in Human Artifact Dataset.

HandCraft [38] both use post-processing techniques with ControlNet [60], conditioning on hand mesh models, shape, and depth masks to correct malformed hands. Hand-to-Diffusion [36] and HanDiffuser [28] adopt end-to-end approaches that integrate hand generation directly into the synthesis pipeline, conditioning on detailed hand-related parameters, focus solely on human image generation. However, with arbitrary images, all these methods are unable to assess hand artifacts by severity. In contrast, extending beyond hand-specific artifacts, our HADM not only detects various types of human artifacts but also supports further improvements through diffusion model finetuning and human artifact correction by inpainting.

### 3. Human Feedback for Human Artifacts

#### 3.1. Dataset Overview

##### 3.1.1 Prompt and Image Collection Pipeline

We collect prompts from GPT-4 [32] and generate samples using four advanced text-to-image models: SDXL [37], DALLE-2 [30], DALLE-3 [31], and Midjourney [12]. For prompt generation, GPT-4 is queried to produce diverse prompts focused on humans in various backgrounds, activities, and framing styles. A total of 4,426 prompts are collected and divided into 90% for the training set and 10% for the validation set. Using these prompts, images are generated via SDXL with different random seeds. A subset of the prompts is also used to generate samples from DALLE-2, DALLE-3, and Midjourney. In total, 25,565 samples are collected from SDXL, 1,605 from DALLE-2, 2,419 from DALLE-3, and 7,965 from Midjourney. Additionally, for diffusion models finetuning, we generate 3,260 prompts for the training set and 255 for the validation set. More details are available in the appendix.

##### 3.1.2 Annotation Pipeline

During the annotation process, annotators are tasked with identifying and marking artifacts using bounding boxes. Example annotations are shown in Fig. 2. After visually inspecting sample images with human artifacts from all four

generators, we empirically observe that many artifacts frequently occur at the extremities of human bodies, necessitating a finer granularity in category definition. Consequently, we divide the human body into six parts: *face*, *torso*, *arm*, *hand*, *leg*, and *feet*, and classify structural inconsistencies in the images as either local or global artifacts. For **local artifacts**, annotators label specific body parts, as defined above, that they consider poorly generated. For instance, in Fig. 2a, the right hand has unusually long fingers with strange textures, and the arm and leg exhibit texture issues on the muscle. Similarly, in Fig. 2b, the face of the left human figure and the hand of the right human figure appear distorted. **Global artifacts** involve broader anatomical inconsistencies that affect the entire human figure, such as extra or missing one or more of the six defined parts (excluding cases of reasonable occlusion or those explicitly specified by textual prompts). These artifacts are grouped into a total of 12 classes. Due to the difficulty of pinpointing specific affected areas in such cases, annotators are instructed to mark the entire human figure. For example, in Fig. 2c, the middle human figure is generated with an extra face, torso, and arm, while the right human figure appears to have an extra leg. Similarly, in Fig. 2d, the highlighted human figure has three arms and hands. Note that multiple class labels may share the same bounding box.

##### 3.1.3 Dataset Statistics

We summarize the data from our Human Artifact Dataset after collecting the prompts, generated images, and annotations. The training set includes 33,374 images with 67,685 local artifacts annotated with bounding boxes and 8,766 global artifacts. The validation set comprises 4,180 images with 7,528 local artifacts annotated with bounding boxes and 873 global artifacts. Fig. 3 presents a detailed breakdown of the annotations for various artifact classes across the four image generators included in HAD.

### 3.2. Model Overview

To optimize performance while maintaining generalizability, we utilize the off-the-shelf ViTDet model [19] with

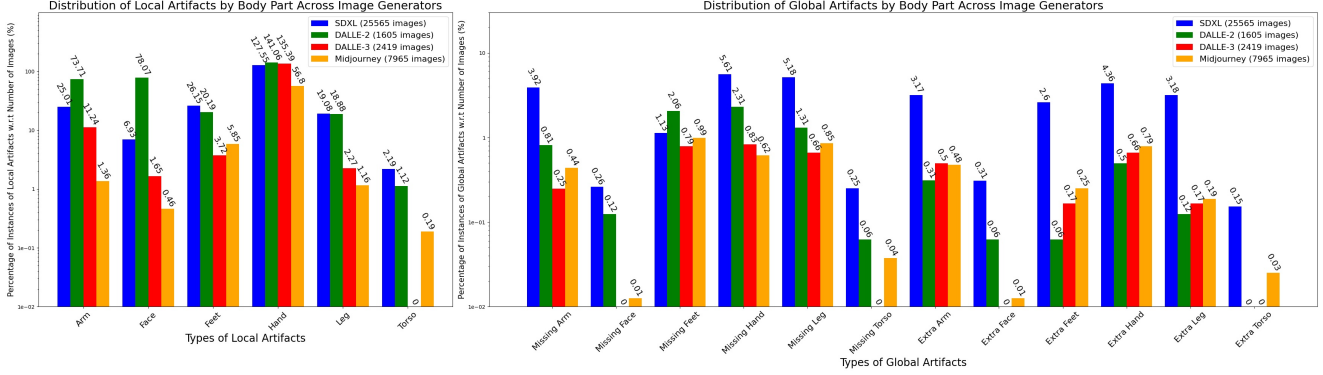


Figure 3. Distribution of local (left) and global (right) artifacts by categories across four different image generators in our Human Artifact Dataset. From the figure, several key observations emerge: Local artifacts are significantly more common than global artifacts, particularly in the hands, across all generators. Generator-wise, SDXL produces the highest number of global artifacts, while DALLE-2 produces the highest number of local artifacts. Both DALLE-3 and Midjourney exhibit stronger human structural coherence, with fewer overall artifacts. DALLE-3 shows a slight advantage in avoiding global artifacts, whereas Midjourney performs marginally better in avoiding local artifacts.

EVA-02 [4] as the backbone and Cascade-RCNN [2] as the detection head. Due to the differing nature of the local and global artifacts we defined, we train two separate models: **Local Human Artifact Detection Model (HADM-L)** for local artifacts and **Global Human Artifact Detection Model (HADM-G)** for global artifacts. HADM-L is a standard object detection model trained on images annotated with six types of local artifacts, each with corresponding bounding boxes, while HADM-G is designed to handle a multi-label object detection task. To accommodate this, we use binary cross-entropy loss to independently model the 12 categories. To improve robustness and reduce false positives on higher-quality generated body parts, we incorporate a broad range of real human datasets for different tasks, including human parsing [18], human instance segmentation [62], human detection [43, 46], and human interaction recognition [49], as well as the COCO dataset [21]. These images are included in the training process with empty annotations, ensuring the models learn to differentiate between realistic human body parts and those with artifacts.

### 3.3. Finetuning Diffusion Models with Guidance from HADM

To demonstrate the application of HADM, we employ LoRA[10] to finetune SDXL [37] on newly generated images using predictions from HADM. Specifically, we generate images from the training set of the prompts for diffusion model finetuning, as described in Sec. 3.1.1. Once the images are generated, we apply HADM to detect local and global artifacts. We then select the top  $k\%$  of predicted bounding boxes from each category to identify artifacts. During finetuning, we use the original prompt as the caption for generated images. For each identified artifact, we prepend “weird [ARTIFACT-TYPE]” to the prompt as a special identifier. At inference, these identifiers serve as negative prompts to prevent artifact generation and are ap-

plied to both the original and finetuned models for evaluation. Additionally, we incorporate images from COCO [21] along with corresponding prompts as regularization to prevent the model from deviating aggressively from the original weights while improving human structural coherence.

## 4. Experiments

The performance and robustness of our HADM are assessed on both in-domain and out-of-domain data. In-domain data includes the images from the validation set of HAD, while out-of-domain data includes images generated by Stable Diffusion 1.4 [40], PixArt- $\Sigma$  [3], FLUX.1-dev [15], and the real human dataset 300W [41]. Experiment settings and details are provided in the appendix.

### 4.1. Quantitative Results

**Local Human Artifact Detection Model:** To evaluate the model’s performance, we use the AP50 metric. The results for HADM-L are shown in Tab. 1. We observe that generators with a higher frequency of human artifacts, such as SDXL and DALLE-2, achieve higher AP50 scores compared to more advanced generators like DALLE-3 and Midjourney. Furthermore, categories with more frequent artifacts, such as *hand* and *feet*, achieve higher AP50 scores compared to less common categories like *torso* and *leg*.

**Global Human Artifact Detection Model:** The results for HADM-G are provided in Tab. 2. Compared to HADM-L, the limited number of global artifact annotations leads to lower overall performance. Among the generators, HADM-G shows comparatively better performance on SDXL, which has the majority of global artifact annotations. In contrast, DALLE-2, despite strong performance in detecting local artifacts and abundant local annotations, performs worse in detecting global artifacts, likely due to fewer annotations available for this task. Further discussion and analysis of these results can be found in Sec. 4.2.

Table 1. Local Detection Results. Each cell shows the AP50 score / number of instances in the val set.

Domain	Face	Torso	Arm	Hand	Leg	Feet	Average
SDXL	26.0 / 238	26.8 / 39	25.4 / 672	80.1 / 3493	28.8 / 477	50.0 / 672	39.5
DALLE-2	86.6 / 145	100.0 / 1	52.7 / 131	88.9 / 228	39.4 / 36	56.8 / 42	70.7
DALLE-3	2.7 / 7	- / 0	8.8 / 46	48.2 / 563	7.4 / 10	20.0 / 27	17.4
Midjourney	5.5 / 4	- / 0	9.8 / 22	54.4 / 586	14.0 / 13	27.8 / 51	22.3
ALL	53.4 / 398	27.6 / 43	28.9 / 875	74.5 / 4875	28.1 / 539	47.3 / 798	43.3

Table 2. Global Detection Results. Each cell shows the AP50 score / number of instances in the val set.

Domain	Missing Artifacts						Extra Artifacts						Average
	Face	Torso	Arm	Hand	Leg	Feet	Face	Torso	Arm	Hand	Leg	Feet	
SDXL	6.7 / 6	7.7 / 6	0.0 / 4	0.0 / 2	23.5 / 93	39.9 / 77	29.9 / 123	40.1 / 112	35.2 / 113	51.9 / 71	41.5 / 142	52.2 / 55	27.4
DALLE-2	- / 0	- / 0	- / 0	- / 0	0.0 / 1	- / 0	0.0 / 1	- / 0	14.3 / 2	- / 0	16.7 / 1	0.0 / 1	6.2
DALLE-3	- / 0	- / 0	0.0 / 1	- / 0	- / 0	33.3 / 7	33.3 / 1	33.3 / 9	11.3 / 2	- / 0	6.8 / 3	- / 0	19.7
Midjourney	- / 0	- / 0	- / 0	- / 0	1.9 / 5	6.3 / 2	3.4 / 6	20.5 / 4	24.0 / 7	0.0 / 2	22.6 / 8	8.4 / 3	10.9
ALL	5.2 / 6	2.4 / 6	0.0 / 5	0.0 / 2	21.0 / 101	38.2 / 86	26.9 / 133	38.5 / 125	32.0 / 123	42.9 / 73	37.5 / 154	41.7 / 59	23.9

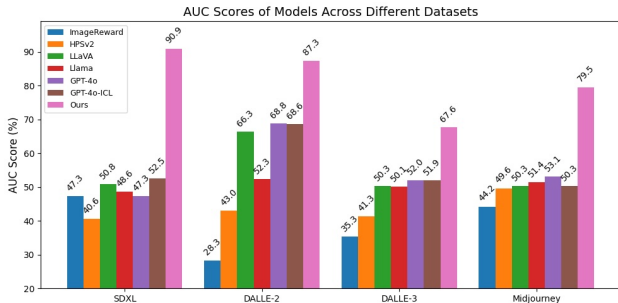


Figure 4. Comparison of the AUC scores of HADM against baseline methods. ICL represents in-context learning.

**Comparison to Baselines:** We compare HADM against publicly available state-of-the-art methods in aesthetics evaluation, specifically HPS-v2 [53] and ImageReward [55]. While these models do not explicitly evaluate human structural coherence, we include them as baselines due to a presumed correlation between aesthetic quality and human structural coherence. Additionally, we test three competitive large vision-language models: GPT-4o [33], LLaVA-1.6-vicuna-13B [23], and Llama-3.2-11B [27].

Since these baselines do not predict bounding boxes, we reframe our detection task as a classification problem. Images in our validation set annotated with any global or local artifacts are labeled as positive, while the rest are labeled negative, resulting in 2,917 positive and 1,263 negative samples. For testing, HPS-v2 and ImageReward produce scalar scores representing preference, while GPT-4o, LLaVA-1.6, and Llama-3.2 are instructed to rate human-related artifacts on a scale from 1 (no artifact) to 5 (catastrophic artifact). We also test GPT-4o with in-context learning, providing it with four sample images with their human

artifacts highlighted before prompting for predictions. For HADM, we use the highest score among all bounding boxes marked as human artifacts as the image’s final score.

We use the AUC score as the evaluation metric to assess the models’ ability to rank the severity of human artifacts in images. As shown in Fig. 4, both aesthetics-focused methods achieve AUC scores below 50%, indicating a weak or even negative correlation between aesthetic evaluation and human artifact detection. This result suggests that while aesthetics and human structural coherence may appear related, these baselines are inadequate for identifying human artifacts. For vision-language models, GPT-4o and LLaVA perform better on images generated by DALLE-2, which has a higher prevalence of local artifacts, as highlighted in Fig. 3 and Tab. 1. This finding indicates that these models have a limited capacity to detect obvious artifacts, particularly from less sophisticated generators. However, their AUC scores drops to near 50% when tested on more advanced generators. Furthermore, we find that the in-context learning setup does not improve artifact identification, highlighting the inherent challenges of this task. In contrast, our HADM significantly outperforms all baselines across all datasets, underscoring its effectiveness in detecting human-related artifacts in generated images.

## 4.2. Discussion

**In-Domain Performance:** To analyze failure cases, we examine high-confidence false positives, as visualized in Fig. 5. We find that some errors appear to stem from occasional oversight by annotators. For example, the distorted face in Fig. 5a and the extra arms in Fig. 5b are overlooked, likely because they appear in a less prominent area of the image. We also notice subjective ambiguity in some re-



Figure 5. Examples of predictions from our HADM considered mistakes during evaluation on SDXL (a), DALLE-3 (b), DALLE-2 (c), and Midjourney (d). FP: false positive, FN: false negative. Red bounding boxes represent the detected artifact with top prediction scores, blue bounding boxes represent other detected bounding boxes with the same class label.

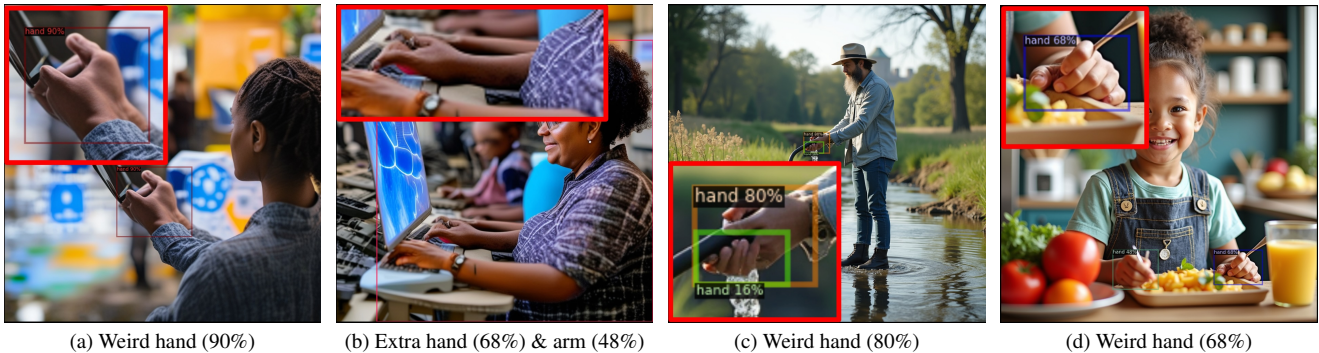


Figure 6. (a), (b): Top predictions of HADM on PixArt- $\Sigma$ . (c), (d): Top predictions of HADM on FLUX.1-dev.

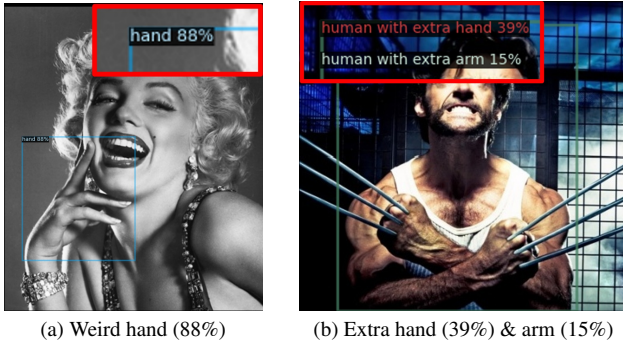


Figure 7. Top predictions of HADM on real images from 300W.

gions, where their severity is difficult for annotators to assess. For instance, HADM detect extra hands in Fig. 5c and Fig. 5d, which are missed by annotators. We consider these as corner cases, as the seemingly extra hands could also be interpreted as belonging to other human figures, albeit with very high uncertainty. Overall, visual inspection verifies our models’ robustness, demonstrating that they can still make reasonable predictions under challenging conditions.

**Performance Discrepancy Among Generators:** We investigate the reasons behind the significant performance gaps in our detection models across different domains, as shown in Tab. 1 and Tab. 2. For instance, DALLE-3 and

Midjourney consistently achieve lower AP50 scores compared to the two legacy models, and there is a notable discrepancy between the performance of local and global human artifacts on DALLE-2. To better understand these differences, we conduct a deeper analysis of the predictions made by our models. We observe a higher proportion of ambiguous cases, similar to those illustrated in Fig. 5c and Fig. 5d, in datasets from generators that produce high-quality human images, where annotations are sparse. This trend aligns with the data distribution shown in Fig. 3. Such results are expected, as advanced generators like DALLE-3, Midjourney, and DALLE-2 (for global artifacts) produce images with relatively stronger human structural coherence. Consequently, these generators result in fewer and subtler artifacts, which are harder to distinguish. With fewer artifact instances available for evaluation, ambiguous cases make up a larger proportion, exerting a stronger influence on overall accuracy and ultimately lowering reported performance. We believe this explains the performance discrepancy among different generators observed in Tab. 1 and Tab. 2. Additional results are provided in the appendix.

**Performance on Unseen Domains:** To assess the performance of HADM on unseen domains, we generate images using the validation set of the finetuning prompts introduced in Sec. 3.1.1 with three impactful image generators: Sta-



Figure 8. Examples of the original SDXL (first row) vs. our finetuned model (second row).

Table 3. Statistics of scores from HADM on different datasets.

Dataset (# of Samples)	Local		Global	
	Number	Mean / Median	Number	Mean / Median
SD1.4 [40] (255)	2426	0.40 / 0.30	119	0.15 / 0.10
PixArt- $\Sigma$ [3] (255)	414	0.35 / 0.32	58	0.22 / 0.15
Flux.1-dev [15] (255)	115	0.26 / 0.24	0	0.00 / 0.00
300W [41] (600)	62	0.28 / 0.23	4	0.26 / 0.25

ble Diffusion 1.4 (SD1.4) [40], PixArt- $\Sigma$  [3], and FLUX.1-dev [15]. We also evaluate our models’ robustness on the real human portrait dataset 300W [41].

We present the top predictions from HADM on the generated images in Fig. 6 and on 300W in Fig. 7. Additional results for SD1.4 and other domains are provided in the appendix. For images from PixArt- $\Sigma$ , HADM-L accurately identifies a hand with an unusual shape in Fig. 6a, while HADM-G detects subtle global artifacts, such as an extra hand and an extra arm in 6b. For images generated by the more advanced FLUX.1-dev model, which generally produces higher-quality images with fewer artifacts, HADM-L still identifies nuanced issues, including a right hand with odd positioning and texture in Fig. 6c, and a hand with an extra finger in Fig. 6d. These results highlight the ability of our model to detect subtle issues across diverse and complex scenarios, including those from unseen, more sophisticated generators. For the real human dataset 300W, HADM-L detects the hand in Fig. 7a. We attribute this to the image’s distinctive black-and-white style, which is rare in the training data from generative models, as well as the

complex hand pose, a feature often associated with artifacts in our training data. In the case of global artifacts, HADM-G produces an interesting result by incorrectly identifying Wolverine’s claw as an extra hand, as shown in Fig. 7b.

To provide a more comprehensive analysis, we compute the models’ output statistics across all domains, presented in Tab. 3. The table shows a general decrease in the number of predictions and confidence scores as the generator quality improves with more advanced models. When tested on real images, although a few predictions are influenced by the aforementioned domain gap issue, our models still produce fewer predictions compared to those for generated images. In summary, these results validate the reliability and robustness of our models across diverse domains, effectively identifying both local and global artifacts, even in challenging scenarios.

## 5. Improvement from Feedback of Human Artifacts Detection

### 5.1. Finetuning Diffusion Models

**Experiment Details** For better generalization, each finetuning prompt is diversified using Llama-3.2-3B [27] with a temperature of 2, generating 10 unique prompts per original prompt. From each diversified prompt, we generate 3 images. We then select the top  $k = 30\%$  of the predicted bounding boxes based on confidence scores to identify artifacts. During training, both the VAE and the text encoder remain frozen, while LoRA is configured with a rank of 32.

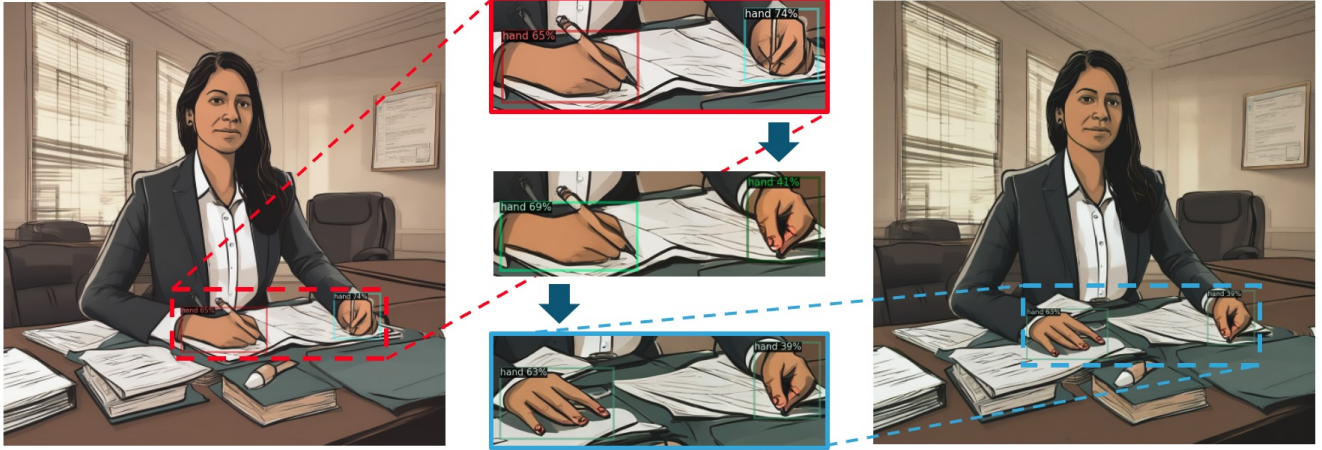


Figure 9. Workflow illustrating the reduction of human artifacts through iterative inpainting. Starting with the initial image (left), we identify artifacts using HADM-L. These artifacts are iteratively corrected by applying inpainting to the top predictions within the corresponding bounding boxes. For each bounding box, multiple inpainting operations are performed in parallel using different random seeds. From these results, HADM-L is reapplied, and the sample with the lower confidence score is selected for each result (middle). This iterative process integrates HADM-L into the inpainting pipeline, automating artifact correction and producing a refined final image (right).

The LoRA weights are trained over 80,000 iterations using the AdamW optimizer [24], with a constant learning rate of  $1 \times 10^{-5}$  and a weight decay of  $1 \times 10^{-2}$ . Our experiments use a batch size of 8. For inference, we run the diffusion process in 50 steps.

**Qualitative results** We present pairs of images generated from the same prompt by both the original SDXL model and our finetuned model in Fig. 8. As shown, our finetuned model effectively reduces severe human artifacts, both local and global, across diverse scenarios and styles. To further assess image quality, we conduct a user preference study involving 15 participants. Images are generated from the validation set of diversified finetuning prompts for both models. Using ViTPose [56], we filter for large, clearly identifiable human figures and randomly select 200 pairs. In each pair, participants are asked to select the image with fewer or less severe human artifacts, avoiding ties whenever possible. Results are presented in Tab. 4, indicating a preference for images from our finetuned model regarding human artifacts. This suggests that, while completely eliminating human artifacts remains challenging, even for advanced diffusion models, our approach effectively mitigates these issues by leveraging predictions from HADM to guide diffusion models in recognizing and avoiding typical human artifacts.

## 5.2. Refining Artifacts via Inpainting

In addition to finetuning, we demonstrate that our HADM-L can be utilized to correct local artifacts in arbitrary images via inpainting, similar to applications as presented in previous works [58, 59]. The pipeline is illustrated in Fig. 9. We adopt SDXL Inpainting-0.1 as the inpainting model in our experiment, setting the guidance scale to 8.0, the inpainting strength to 0.99, and the number of inference steps

Table 4. User preference on original SDXL vs. finetuned SDXL: the percentage of examples where original SDXL is significantly worse ( $\ll$ ), slightly worse ( $<$ ), about the same ( $\approx$ ), slightly better ( $>$ ), significantly better ( $\gg$ ) than finetuned SDXL.

Preference	$\ll$	$<$	$\approx$	$>$	$\gg$
%	29.00	26.00	6.30	21.57	17.13

to 30. For each detected artifact, we apply inpainting with 20 different random seeds and select the result based on HADM-L’s confidence scores. We note that increasing the number of random seeds generally results in a more thorough search, improving the likelihood of obtaining better results, albeit at the cost of additional time and computational resources. More results and discussions are available in the appendix.

## 6. Conclusion

In this work, we introduce a comprehensive approach for detecting and mitigating human artifacts in images generated by text-to-image models. By curating Human Artifact Dataset (HAD), the first large-scale dataset with detailed annotations of local and global human artifacts, we establish a foundation for training Human Artifact Detection Models (HADM) to detect these artifacts. Our experiments demonstrate that HADM not only accurately identify diverse human artifacts across multiple domains but also effectively generalize to images from unseen generative models outside the training data. Furthermore, we highlight the application and potential of our approach by showing how HADM’s predictions can guide the finetuning of diffusion models and enhance inpainting workflows, effectively reducing human artifacts in generated images.



**Acknowledgments** We thank Boqing Gong for providing valuable feedback.

**Ethical Considerations** Our experiments demonstrate the robustness of HADM in real-world scenarios; however, we emphasize that our models are designed solely for evaluating synthetic images generated by text-to-image models. We strongly discourage applying this model to real-human images, as it may produce unintended or inappropriate interpretations, particularly for individuals with unique health conditions or physical characteristics. Such misapplications could result in unethical or harmful consequences.

## References

- [1] Tim Brooks, Aleksander Holynski, and Alexei A. Efros. Instructpix2pix: Learning to follow image editing instructions. In *CVPR*, pages 18392–18402, 2023. 1
- [2] Zhaowei Cai and Nuno Vasconcelos. Cascade R-CNN: delving into high quality object detection. In *CVPR*, pages 6154–6162, 2018. 4, 1
- [3] Junsong Chen, Chongjian Ge, Enze Xie, Yue Wu, Lewei Yao, Xiaozhe Ren, Zhongdao Wang, Ping Luo, Huchuan Lu, and Zhenguo Li. Pixart- $\Sigma$ : Weak-to-strong training of diffusion transformer for 4k text-to-image generation. *CoRR*, abs/2403.04692, 2024. 4, 7
- [4] Yuxin Fang, Quan Sun, Xinggang Wang, Tiejun Huang, Xinlong Wang, and Yue Cao. EVA-02: A visual representation for neon genesis. *Image and Vision Computing*, page 105171, 2024. 4, 1
- [5] Oran Gafni, Adam Polyak, Oron Ashual, Shelly Sheynin, Devi Parikh, and Yaniv Taigman. Make-a-scene: Scene-based text-to-image generation with human priors. In *ECCV*, pages 89–106, 2022. 1, 2
- [6] Hasan Abed Al Kader Hammoud, Hani Itani, Fabio Pizzati, Philip Torr, Adel Bibi, and Bernard Ghanem. Synthclip: Are we ready for a fully synthetic CLIP training? *CoRR*, abs/2402.01832, 2024. 1
- [7] Jack Hessel, Ari Holtzman, Maxwell Forbes, Ronan Le Bras, and Yejin Choi. Clipscore: A reference-free evaluation metric for image captioning. In *EMNLP*, pages 7514–7528, 2021. 2
- [8] Martin Heusel, Hubert Ramsauer, Thomas Unterthiner, Bernhard Nessler, and Sepp Hochreiter. Gans trained by a two time-scale update rule converge to a local nash equilibrium. In *NeurIPS*, pages 6626–6637, 2017. 2
- [9] Jonathan Ho, Ajay Jain, and Pieter Abbeel. Denoising diffusion probabilistic models. In *NeurIPS*, 2020. 2
- [10] Edward J. Hu, Yelong Shen, Phillip Wallis, Zeyuan Allen-Zhu, Yuanzhi Li, Shean Wang, Lu Wang, and Weizhu Chen. Lora: Low-rank adaptation of large language models. In *ICLR*. OpenReview.net, 2022. 4
- [11] Kaiyi Huang, Kaiyue Sun, Enze Xie, Zhenguo Li, and Xihui Liu. T2I-CompBench: A comprehensive benchmark for open-world compositional text-to-image generation. In *NeurIPS*, 2023. 2
- [12] Midjourney Inc. Midjourney. <https://www.midjourney.com/>, 2023. 1, 2, 3
- [13] Bahjat Kawar, Shiran Zada, Oran Lang, Omer Tov, Huiwen Chang, Tali Dekel, Inbar Mosseri, and Michal Irani. Imagic: Text-based real image editing with diffusion models. In *CVPR*, pages 6007–6017, 2023. 1
- [14] Yuval Kirstain, Adam Polyak, Uriel Singer, Shahbuland Matiana, Joe Penna, and Omer Levy. Pick-a-pic: An open dataset of user preferences for text-to-image generation. In *NeurIPS*, 2023. 2
- [15] Black Forest Lab. Flux. <https://blackforestlabs.ai/>, 2023. 1, 4, 7
- [16] Tony Lee, Michihiro Yasunaga, Chenlin Meng, Yifan Mai, Joon Sung Park, Agrim Gupta, Yunzhi Zhang, Deepak Narayanan, Hannah Teufel, Marco Bellagente, Minguk Kang, Taesung Park, Jure Leskovec, Jun-Yan Zhu, Fei-Fei Li, Jiajun Wu, Stefano Ermon, and Percy Liang. Holistic evaluation of text-to-image models. In *NeurIPS*, 2023. 2
- [17] Baiqi Li, Zhiqiu Lin, Deepak Pathak, Jiayao Li, Yixin Fei, Kewen Wu, Tiffany Ling, Xide Xia, Pengchuan Zhang, Graham Neubig, and Deva Ramanan. GenAI-Bench: Evaluating and improving compositional text-to-visual generation. *CoRR*, abs/2406.13743, 2024. 2
- [18] Jianshu Li, Jian Zhao, Yunchao Wei, Congyan Lang, Yidong Li, and Jiashi Feng. Towards real world human parsing: Multiple-human parsing in the wild. *CoRR*, abs/1705.07206, 2017. 4
- [19] Yanghao Li, Hanzi Mao, Ross B. Girshick, and Kaiming He. Exploring plain vision transformer backbones for object detection. In *ECCV*, pages 280–296, 2022. 3
- [20] Youwei Liang, Junfeng He, Gang Li, Peizhao Li, Arseniy Klimovskiy, Nicholas Carolan, Jiao Sun, Jordi Pont-Tuset, Sarah Young, Feng Yang, Junjie Ke, Krishnamurthy Dj Divijotham, Katie Collins, Yiwen Luo, Yang Li, Kai J. Kohlhoff, Deepak Ramachandran, and Vidhya Navalpakkam. Rich human feedback for text-to-image generation. *CVPR*, pages 19401–19411, 2024. 2
- [21] Tsung-Yi Lin, Michael Maire, Serge J. Belongie, James Hays, Pietro Perona, Deva Ramanan, Piotr Dollár, and C. Lawrence Zitnick. Microsoft COCO: common objects in context. In *ECCV*, pages 740–755, 2014. 4
- [22] Zhiqiu Lin, Deepak Pathak, Baiqi Li, Jiayao Li, Xide Xia, Graham Neubig, Pengchuan Zhang, and Deva Ramanan. Evaluating text-to-visual generation with image-to-text generation. In *ECCV*, pages 366–384, 2024. 2
- [23] Haotian Liu, Chunyuan Li, Yuheng Li, Bo Li, Yuanhan Zhang, Sheng Shen, and Yong Jae Lee. Llava-next: Improved reasoning, ocr, and world knowledge, 2024. 1, 5
- [24] Ilya Loshchilov and Frank Hutter. Decoupled weight decay regularization. In *ICLR*, 2019. 8, 1
- [25] Wenquan Lu, Yufei Xu, Jing Zhang, Chaoyue Wang, and Dacheng Tao. Handrefiner: Refining malformed hands in generated images by diffusion-based conditional inpainting. *CoRR*, abs/2311.17957, 2023. 2
- [26] Elman Mansimov, Emilio Parisotto, Lei Jimmy Ba, and Ruslan Salakhutdinov. Generating images from captions with attention. In *ICLR*, 2016. 1, 2
- [27] Meta. Llama 3.2. <https://ai.meta.com/blog/llama-3-2-connect-2024-vision-edge-mobile-devices/>, 2024. 5, 7, 1

- [28] Supreeth Narasimhaswamy, Uttaran Bhattacharya, Xiang Chen, Ishita Dasgupta, Saayan Mitra, and Minh Hoai. Hand-iffuser: Text-to-image generation with realistic hand appearances. In *CVPR*, pages 2468–2479, 2024. 3
- [29] Alexander Quinn Nichol, Prafulla Dhariwal, Aditya Ramesh, Pranav Shyam, Pamela Mishkin, Bob McGrew, Ilya Sutskever, and Mark Chen. Glide: Towards photorealistic image generation and editing with text-guided diffusion models. In *ICML*, pages 16784–16804, 2022. 2
- [30] OpenAI. DALL-E 2. <https://openai.com/index/dall-e-2/>, 2022. 1, 2, 3
- [31] OpenAI. DALL-E 3. <https://openai.com/index/dall-e-3/>, 2023. 1, 2, 3
- [32] OpenAI. GPT-4. <https://openai.com/index/gpt-4/>, 2023. 3
- [33] OpenAI. GPT-4o. <https://openai.com/index/hello-gpt-4o/>, 2024. 1, 5
- [34] Mayu Otani, Riku Togashi, Yu Sawai, Ryosuke Ishigami, Yuta Nakashima, Esa Rahtu, Janne Heikkilä, and Shin’ichi Satoh. Toward verifiable and reproducible human evaluation for text-to-image generation. In *CVPR*, pages 14277–14286, 2023. 2
- [35] Gaurav Parmar, Richard Zhang, and Jun-Yan Zhu. On aliased resizing and surprising subtleties in GAN evaluation. In *CVPR*, pages 11400–11410, 2022. 2
- [36] Anton Pelykh, Ozge Mercanoglu Sincan, and Richard Bowden. Giving a hand to diffusion models: A two-stage approach to improving conditional human image generation. In *FG*, pages 1–10, 2024. 3
- [37] Dustin Podell, Zion English, Kyle Lacey, Andreas Blattmann, Tim Dockhorn, Jonas Müller, Joe Penna, and Robin Rombach. SDXL: Improving latent diffusion models for high-resolution image synthesis. In *ICLR*, 2024. 1, 2, 3, 4
- [38] Zhenyue Qin, Yiqun Zhang, Yang Liu, and Dylan Campbell. HandCraft: Anatomically correct restoration of malformed hands in diffusion generated images. *CoRR*, abs/2403.01693, 2024. 3
- [39] Aditya Ramesh, Mikhail Pavlov, Gabriel Goh, Scott Gray, Chelsea Voss, Alec Radford, Mark Chen, and Ilya Sutskever. Zero-shot text-to-image generation. In *ICML*, 2021. 2
- [40] Robin Rombach, Andreas Blattmann, Dominik Lorenz, Patrick Esser, and Björn Ommer. High-resolution image synthesis with latent diffusion models. In *CVPR*, pages 10674–10685, 2022. 1, 2, 4, 7
- [41] Christos Sagonas, Georgios Tzimiropoulos, Stefanos Zafeiriou, and Maja Pantic. 300 faces in-the-wild challenge: The first facial landmark localization challenge. In *ICCV Workshop*, pages 397–403, 2013. 4, 7
- [42] Tim Salimans, Ian J. Goodfellow, Wojciech Zaremba, Vicki Cheung, Alec Radford, and Xi Chen. Improved techniques for training gans. In *NeurIPS*, pages 2226–2234, 2016. 2
- [43] Shuai Shao, Zijian Zhao, Boxun Li, Tete Xiao, Gang Yu, Xiangyu Zhang, and Jian Sun. Crowdhuman: A benchmark for detecting human in a crowd. *CoRR*, abs/1805.00123, 2018. 4
- [44] Shuai Shao, Zeming Li, Tianyuan Zhang, Chao Peng, Gang Yu, Xiangyu Zhang, Jing Li, and Jian Sun. Objects365: A large-scale, high-quality dataset for object detection. In *ICCV*, pages 8429–8438, 2019. 1
- [45] Shelly Sheynin, Adam Polyak, Uriel Singer, Yuval Kirstain, Amit Zohar, Oron Ashual, Devi Parikh, and Yaniv Taigman. Emu edit: Precise image editing via recognition and generation tasks. In *CVPR*, pages 8871–8879, 2024. 1
- [46] Jianping Shi, Renjie Liao, and Jiaya Jia. Codel: a human co-detection and labeling framework. In *ICCV*, pages 2096–2103, 2013. 4
- [47] Krishnakant Singh, Thanush Navaratnam, Jannik Holmer, Simone Schaub-Meyer, and Stefan Roth. Is synthetic data all we need? benchmarking the robustness of models trained with synthetic images. In *CVPRW*, pages 2505–2515, 2024. 1
- [48] Jascha Sohl-Dickstein, Eric A. Weiss, Niru Maheswaranathan, and Surya Ganguli. Deep unsupervised learning using nonequilibrium thermodynamics. In *ICML*, pages 2256–2265, 2015. 2
- [49] Gokhan Tanisik, Cemil Zalluhoglu, and Nazli Ikizler-Cinbis. Facial descriptors for human interaction recognition in still images. *Pattern Recognition Letters*, 73:44–51, 2016. 4
- [50] Ming Tao, Hao Tang, Fei Wu, Xiaoyuan Jing, Bing-Kun Bao, and Changsheng Xu. DF-GAN: A simple and effective baseline for text-to-image synthesis. In *CVPR*, pages 16494–16504, 2022. 1, 2
- [51] Yonglong Tian, Lijie Fan, Phillip Isola, Huiwen Chang, and Dilip Krishnan. StableRep: Synthetic images from text-to-image models make strong visual representation learners. In *NeurIPS*, 2023. 1
- [52] Yonglong Tian, Lijie Fan, Kaifeng Chen, Dina Katabi, Dilip Krishnan, and Phillip Isola. Learning vision from models rivals learning vision from data. In *CVPR*, pages 15887–15898, 2024. 1
- [53] Xiaoshi Wu, Yiming Hao, Keqiang Sun, Yixiong Chen, Feng Zhu, Rui Zhao, and Hongsheng Li. Human preference score v2: A solid benchmark for evaluating human preferences of text-to-image synthesis. *CoRR*, abs/2306.09341, 2023. 2, 5
- [54] Xiaoshi Wu, Keqiang Sun, Feng Zhu, Rui Zhao, and Hongsheng Li. Human preference score: Better aligning text-to-image models with human preference. In *ICCV*, pages 2096–2105, 2023. 2
- [55] Jiazheng Xu, Xiao Liu, Yuchen Wu, Yuxuan Tong, Qinkai Li, Ming Ding, Jie Tang, and Yuxiao Dong. Imagereward: Learning and evaluating human preferences for text-to-image generation. In *NeurIPS*, 2023. 2, 5
- [56] Yufei Xu, Jing Zhang, Qiming Zhang, and Dacheng Tao. Vitpose: Simple vision transformer baselines for human pose estimation. In *NeurIPS*, 2022. 8, 1
- [57] Hui Ye, Xiulong Yang, Martin Takáč, Rajshekhar Sunderraman, and Shihao Ji. Improving text-to-image synthesis using contrastive learning. In *BMVC*, page 154, 2021. 1, 2
- [58] Yu Zeng, Zhe Lin, Jimei Yang, Jianming Zhang, Eli Shechtman, and Huchuan Lu. High-resolution image inpainting with iterative confidence feedback and guided upsampling. In *ECCV*, pages 1–17, 2020. 8

- [59] Lingzhi Zhang, Yuqian Zhou, Connelly Barnes, Sohrab Amirghodsi, Zhe Lin, Eli Shechtman, and Jianbo Shi. Perceptual artifacts localization for inpainting. In *ECCV*, pages 146–164, 2022. [8](#)
- [60] Lvmin Zhang, Anyi Rao, and Maneesh Agrawala. Adding conditional control to text-to-image diffusion models. In *ICCV*, pages 3813–3824, 2023. [3](#)
- [61] Lingzhi Zhang, Zhengjie Xu, Connelly Barnes, Yuqian Zhou, Qing Liu, He Zhang, Sohrab Amirghodsi, Zhe Lin, Eli Shechtman, and Jianbo Shi. Perceptual artifacts localization for image synthesis tasks. In *ICCV*, pages 7545–7556, 2023. [2](#)
- [62] Song-Hai Zhang, Ruilong Li, Xin Dong, Paul L. Rosin, Zixi Cai, Xi Han, Dingcheng Yang, Haozhi Huang, and Shi-Min Hu. Pose2seg: Detection free human instance segmentation. In *CVPR*, pages 889–898, 2019. [4](#)
- [63] Sharon Zhou, Mitchell L. Gordon, Ranjay Krishna, Austin Narcomey, Li Fei-Fei, and Michael S. Bernstein. HYPE: A benchmark for human eye perceptual evaluation of generative models. In *NeurIPS*, pages 3444–3456, 2019. [2](#)
- [64] Minfeng Zhu, Pingbo Pan, Wei Chen, and Yi Yang. DM-GAN: dynamic memory generative adversarial networks for text-to-image synthesis. In *CVPR*, pages 5802–5810, 2019. [1, 2](#)

# Detecting Human Artifacts from Text-to-Image Models

## Supplementary Material

### 7. Configuration Details

#### 7.1. Data Generation Details

For optimal image quality, both the base and refiner models are used during generation. Before annotation, the generated images are filtered by ViTPose [56], a state-of-the-art human keypoint detection model, to ensure the significant presence of humans and to balance the representation of different body parts. The pipeline is illustrated in Fig. 10.

#### 7.2. Training Detection Models

We use Cascade R-CNN [2] with an EVA-02-ViT-L backbone [4] with additional training on O365 dataset [44]. The model is trained with a batch size of 4 and an image resolution of 1024. For optimization, we follow the implementation in EVA-02 and use AdamW [24] with a learning rate of  $1 \times 10^{-5}$  and  $\beta_1 = 0.9$  and  $\beta_2 = 0.999$ . The model is trained for a total of 250,000 steps. During inference, we set the default threshold value of the detection head to 0.05.

#### 7.3. Finetuning Diffusion Models

To enhance generalization, we further diversify the prompts using Llama-3.2-3B [27] before generating images with SDXL. Additionally, we crop artifacts using bounding boxes and assign the same identifiers as captions to help the diffusion model localize artifacts within images.

#### 7.4. Selecting Inpaint Results

Intuitively, we want to avoid generating human body parts with high scores of artifacts. Nevertheless, we find in our study that simply choosing the lowest score detected among the inpainted regions produces suboptimal results. This is because the inpainting model could generate occluded or missing body parts, which leads to a low score or even no prediction from our HADM-L. As we demonstrate in Fig. 11, the inpainting model generates diverse samples given the bounding box and different random seeds.

Although HADM-L successfully identifies different levels of severity of the artifacts on the hand in Fig. 11b, Fig. 11c, and Fig. 11d, some other regions inpainted as a non-hand object (Fig. 11e) or occluded hand (Fig. 11f) are not identified as the typical artifacts and hence get lower scores or even no detection. In this situation, selecting these results with overly low scores may lead to unexpected behavior. Thus, we empirically conclude that the result should be selected with the value closest to half of the original score of the artifact.

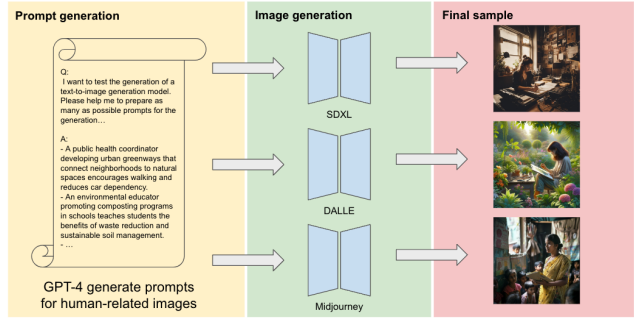


Figure 10. Pipeline of our data collection process.

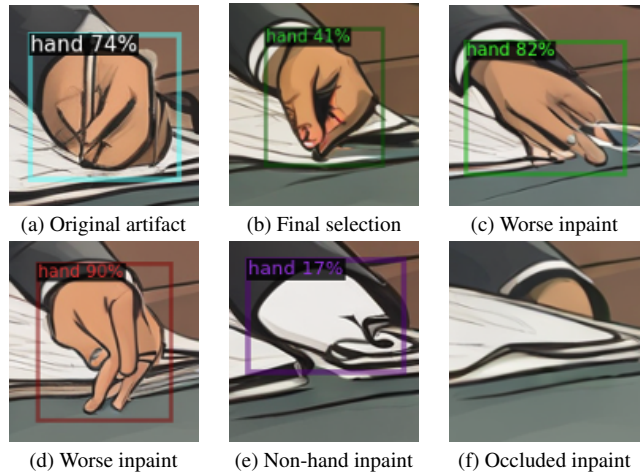


Figure 11. Original artifact and different inpainting results with scores from our HADM-L.

### 8. Ablation Studies

Table 5. Ablation study of key components in HADM-L. AP50 scores are reported, with each additional configuration building upon the previous one.

Config.	ViT-B	+ ViT-L	+ EVA02	+ Real
AP50	32.7	35.3	39.8	43.3

Table 6. Ablation study of key components in HADM-G.

Config.	ViT-B	+ EVA02	+ Real	+ BCE
AP50	14.4	17.7	17.8	25.5

We conduct ablation studies to evaluate the impact of key components in HADM. This includes examining the

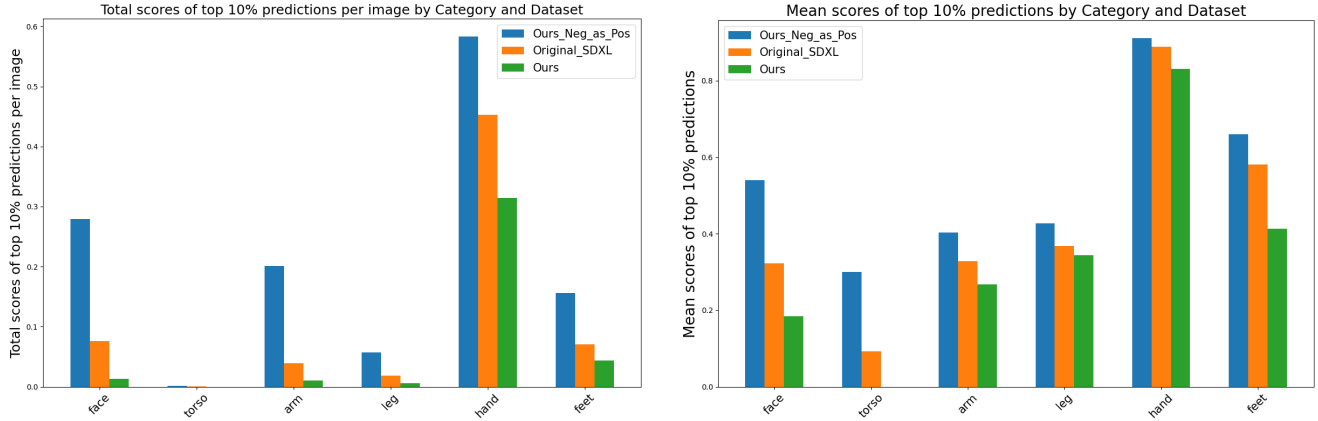


Figure 12. Total scores per image (left) and average scores (right) of top 10% detected local human artifacts.

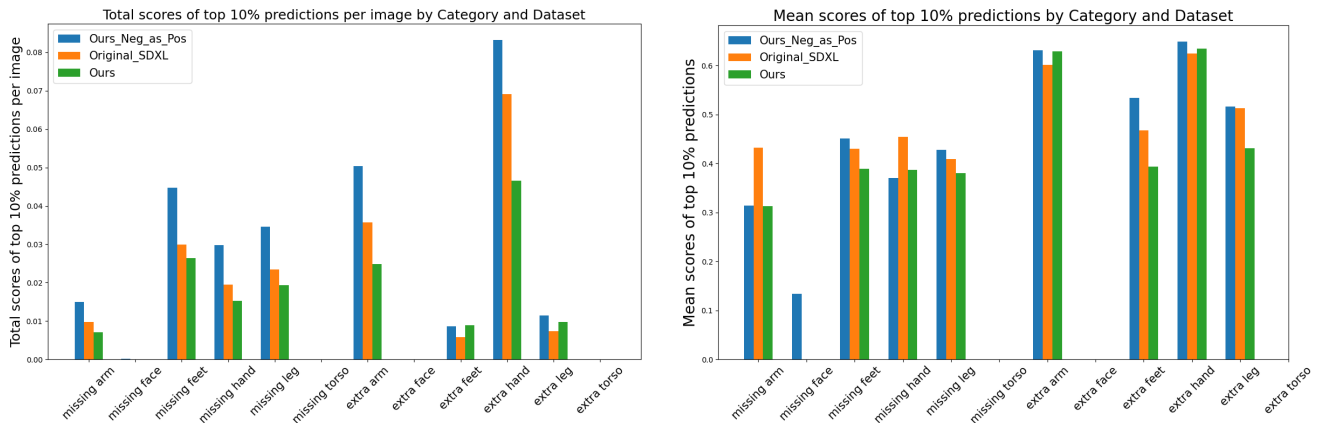


Figure 13. Total scores per image (left) and average scores (right) of top 10% detected global human artifacts.

effect of backbone capacity (ViT-L and EVA02), the use of real-domain regularization images (Real) during training for HADM-L, and the application of binary cross-entropy (BCE) loss for HADM-G. Results for both models are shown in Tables 5 and 6, respectively. As seen in Tab. 5, each enhancement in the backbone architecture results in a clear performance gain, with the inclusion of real-domain images yielding the best performance for HADM-L. In contrast, Tab. 6 shows that while increasing backbone capacity similarly improves the AP50 score, adding real-domain regularization images has minimal impact (+0.1). We attribute this to the limitations of cross-entropy loss in the multi-label setting. Switching to binary cross-entropy loss brings a substantial performance boost (+7.7).

## 9. Quantitative Results for Finetuned Diffusion Models

To more comprehensively evaluate the performance of our finetuned SDXL model, we compare the quantitative detec-

tion results from HADM on images generated by the original and finetuned SDXL models. To further demonstrate the human artifact patterns associated with the special identifiers learned during finetuning, we not only generate images using them as negative prompts but also prepend them to the prompts during inference to generate another set of baseline images for comparison. We then compute the total scores per image and the average scores of the top 10% predictions from HADM-L and HADM-G on the generated images, presenting the results in Fig. 12 and Fig. 13. These results show that, compared to the original SDXL, our finetuned model produces fewer artifacts in terms of both quantity (lower total scores) and quality (lower average scores), which aligns with our user studies. Moreover, when using the identifiers as part of the prompts instead of as negative prompts, the finetuned model generates significantly more human artifacts. This demonstrates the enhanced perception of human artifacts by the finetuned model, validating the effectiveness of our finetuning approach, which benefits from the feedback provided by HADM.



You are an human artifact detector that can help identify artifacts or issues, such as weird/missing/extra face/hand/arm/leg/feet/torso/etc on humans in images. Does this image contain any artifacts on human? Classify the severity of the artifact into the following categories: 1: No human artifact, 2: Minor human artifact, 3: Major human artifact, 4: Critical human artifact, 5: Catastrophic human artifact. If there are multiple artifacts, classify the most severe one. Explain your reasoning.

Based on the provided image and my analysis capabilities, I assess the presence of artifacts and classify their severity as follows:

**Severity Classification: 1 (No human artifact)**

**Reasoning:**

- 1. Human Representation:** The two individuals in the image appear proportionate and complete, with no visible distortions or missing/extra body parts such as arms, legs, or hands.
- 2. Facial Features:** Both individuals' faces seem intact and natural, with no unusual features, misalignment, or "weird" facial anomalies typical of generated artifacts.
- 3. Hands and Interaction:** The hand interaction involving the clipboard is natural and correctly aligned with their actions.
- 4. Context and Environment:** The surroundings are coherent, and no contextual artifacts appear to impact the realism of the scene.

If you have further concerns or need detailed feedback on a specific part of the image, please let me know!

(a) GPT-4o fails to identify any artifacts given the original image without any hint.



Can you observe any abnormality or artifact inside the bounding box I highlighted?

Upon analyzing the region within the highlighted bounding box, I observe the following:

**Artifact Observed**

There is a noticeable distortion or inconsistency in the hand of the individual holding the clipboard. Specifically:

- The hand appears unnaturally shaped or misaligned, with an exaggerated curvature that does not resemble a typical hand anatomy.
- The interaction between the fingers and the clipboard lacks natural depth or clear definition, giving an impression of blending or overlapping errors.

**Severity Classification: 2 (Minor human artifact)**

While the artifact is noticeable upon close examination, it does not significantly impact the overall realism or clarity of the image. It appears as a localized issue rather than a major distortion.

If you'd like, I can provide further analysis or recommendations for addressing such artifacts in the generation process.

(b) When the distorted hand of the right figure is highlighted with a bounding box, GPT-4o recognizes minor artifacts, including the distortion in the hand and its unnatural interaction with objects.



Can you observe any abnormality or artifact inside the bounding box I highlighted?

🌀 Upon inspecting the region within the highlighted bounding box, I observe the following:

#### Artifact Observed

- There is an abnormality in the alignment and shape of the lower hand (the one below the clipboard):
  - The hand appears disproportionately large compared to the natural anatomy.
  - The fingers seem unnaturally positioned or elongated, with an unrealistic structure.
  - The overall positioning of the hand relative to the arm is slightly awkward and lacks a natural flow.

#### Severity Classification: 3 (Major human artifact)

This artifact is more pronounced than the previous one, as the hand's appearance deviates significantly from a natural human anatomy. It could distract from the realism of the image, especially under close inspection.

Let me know if you would like additional analysis or recommendations!

(c) When the three arms of the right figure are highlighted with a bounding box, GPT-4o claims to observe major artifacts but fails to justify the prediction by identifying the three arms.



Can you observe any abnormality or artifact inside the bounding box I highlighted?

🌀 Upon analyzing the region within the highlighted bounding box, I observe the following:

#### Artifact Observed

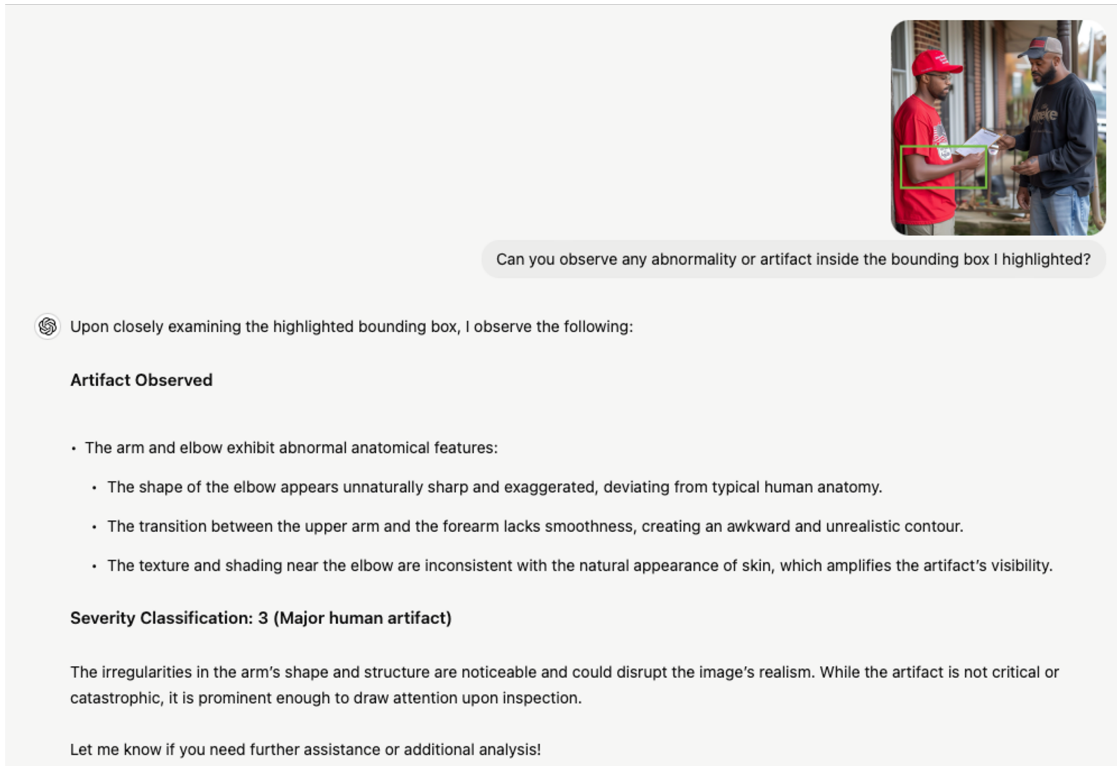
- The hand holding the clipboard exhibits irregularities:
  - The alignment of the fingers seems unnatural, with some appearing to merge or lack clear separation.
  - The thumb is positioned oddly, contributing to an awkward overall hand structure.
  - The interaction with the clipboard looks distorted, as if the hand is not gripping it naturally.

#### Severity Classification: 3 (Major human artifact)

The observed abnormalities in the hand anatomy and its interaction with the clipboard significantly detract from the realism of the image. While not catastrophic, these issues are prominent and could be noticeable even in a casual inspection.

If you'd like further clarification or analysis, feel free to ask!

(d) When the hand of the left figure, which has better quality, is highlighted with a bounding box, GPT-4o still predicts major human artifacts.



(e) When the entire arm of the left figure, which has better quality, is highlighted with a bounding box, GPT-4o still predicts major human artifacts.

Figure 14. Dialogue with GPT-4o providing bounding boxes as hints.

## 10. Testing GPT-4o with more hints

Given GPT-4o’s limited ability to identify, localize, and analyze features within an image, as demonstrated in the main paper, we further evaluate its capacity to recognize artifacts when provided with additional hints, such as bounding boxes. The corresponding dialogue is presented in Fig. 14. The results show that even with localized hints, GPT-4o fails to accurately identify the artifacts or assess their severity. Instead, its behavior appears to conform to the expectations set by the prompt, consistently making positive predictions based on the presence of bounding boxes without providing justification or demonstrating a true understanding of the artifacts.

## 11. Additional Qualitative Examples

**Annotation Examples** We present additional annotation examples of local human artifacts in Fig. 15 and global human artifacts in Fig. 16. These examples reveal that in domains where human artifacts are frequent, such as local artifacts from DALLE-2 and global artifacts from SDXL, the artifacts are generally more obvious and distinguishable. Conversely, in domains where artifacts are rare, such as DALLE-3 and Midjourney, the artifacts tend to be more subtle and ambiguous. These observations align with the

patterns shown in Fig. 3 and the discussion in Sec. 4.2.

**Failure Cases** We present additional results from HADM on the validation set of HAD that are considered incorrect, including false positives and false negatives, in Fig. 17. These results reveal that most of the predictions are reasonable and are classified as errors partly due to occasional oversight by annotators or the growing difficulty in making judgments as the generator’s capacity improves, as discussed in Sec. 4.2.

**Results on Unseen Domains** We present additional results from HADM on images from unseen domains. Our models demonstrate strong generalization to these domains, effectively identifying images generated by both a legacy generator (SD1.4) and more advanced generators (PixArt- $\Sigma$  and FLUX.1-dev). For real images (300W), our models make only a few predictions, primarily due to rare and unusual factors such as atypical poses or challenging lighting conditions.

**Samples from Finetuned SDXL** We present a comparison of images generated by the original and our finetuned SDXL models in Fig. 19. As demonstrated by these images and the quantitative results in Fig. 9, our finetuned SDXL model exhibits a stronger perception of human artifacts, thanks to our finetuning approach that leverages predictions from HADM.



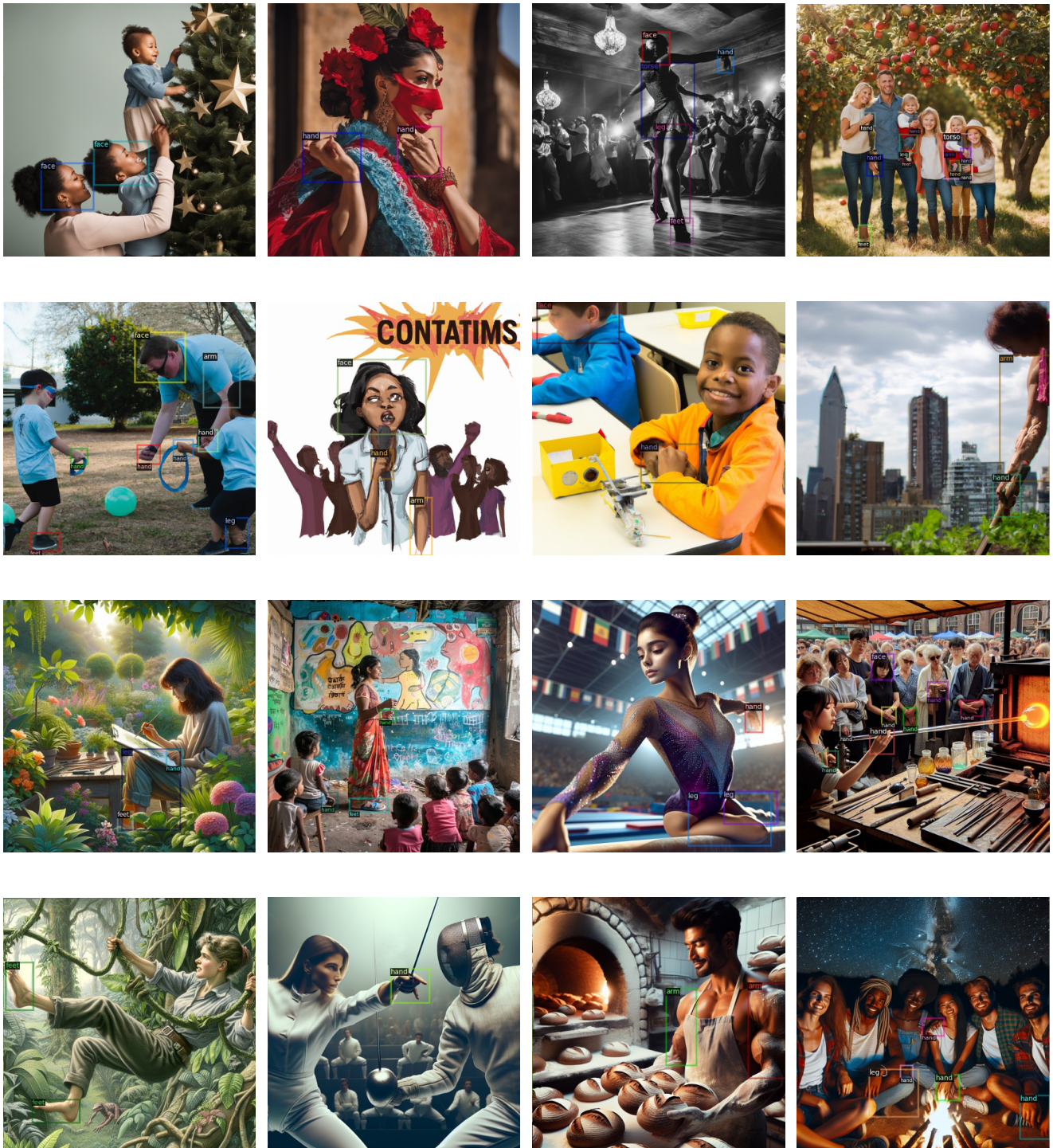


Figure 15. More examples of annotations from Human Artifact Dataset for local human artifacts. First row: SDXL. Second row: DALLE-2. Third row: DALLE-3. Last row: Midjourney.

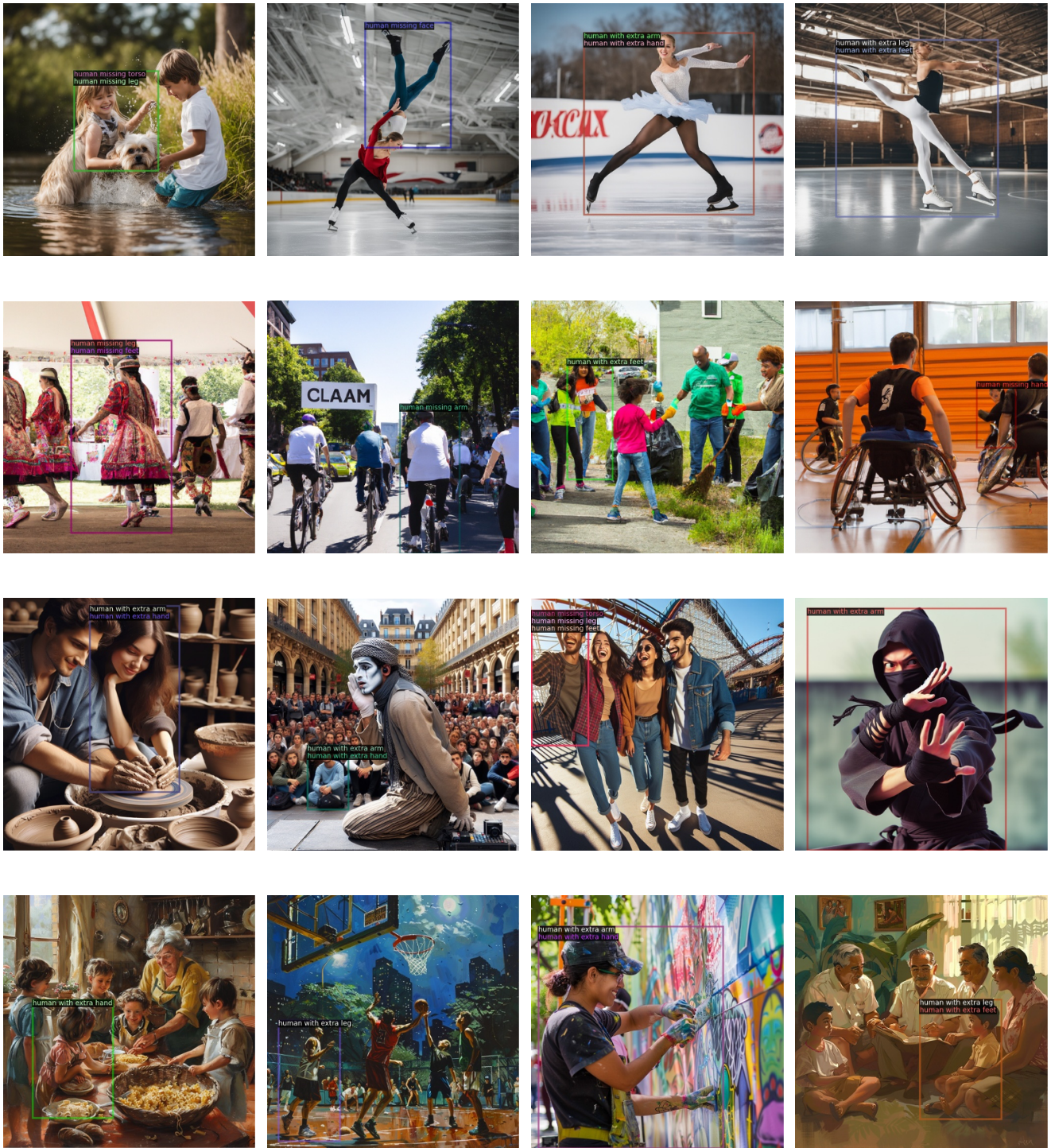


Figure 16. More examples of annotations from Human Artifact Dataset for global human artifacts. First row: SDXL. Second row: DALLE-2. Third row: DALLE-3. Last row: Midjourney.

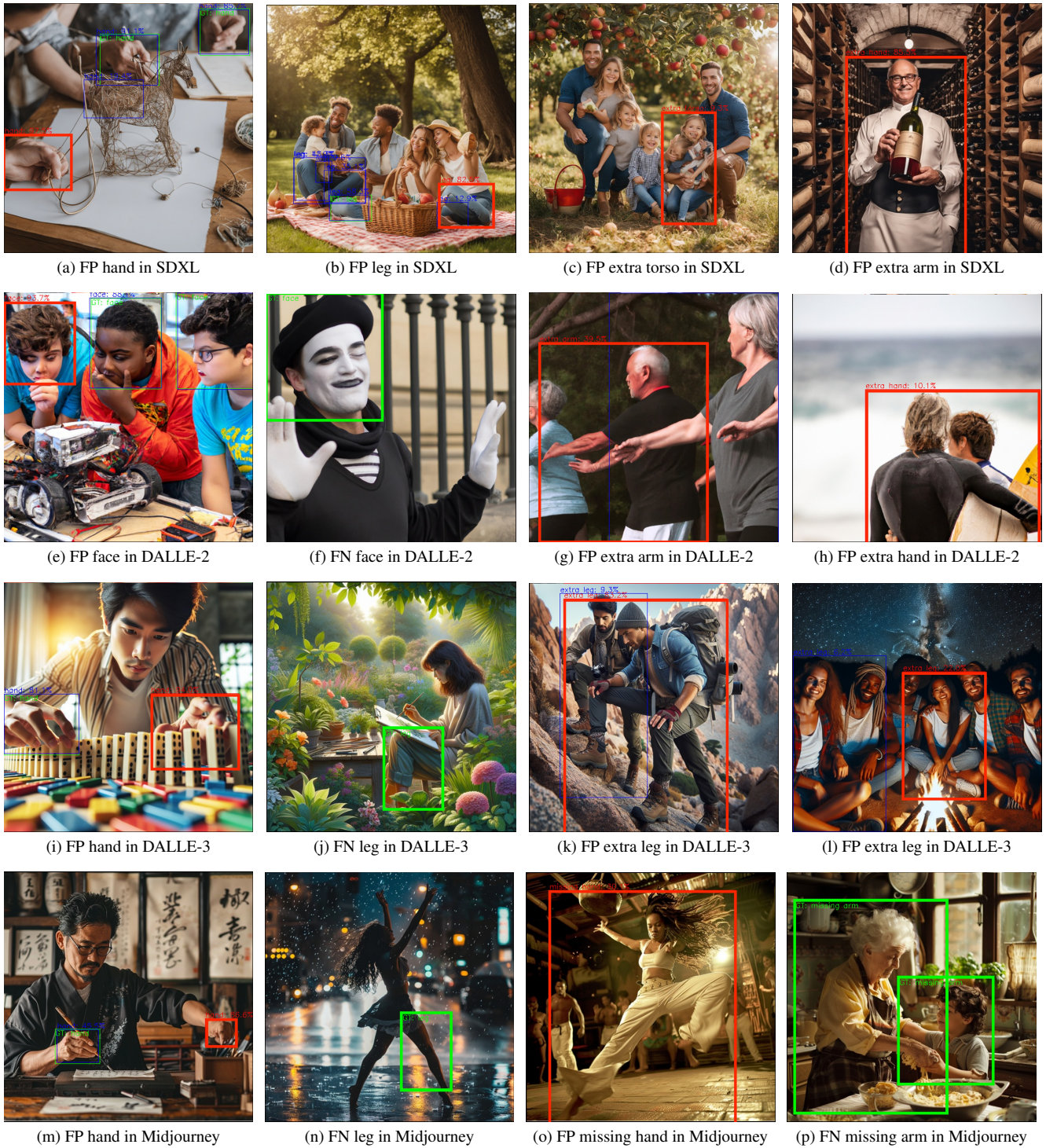


Figure 17. Examples of predictions from our HADM considered mistakes during evaluation on SDXL (first row), DALLE-2 (second row), DALLE-3 (third row), and Midjourney (last row). FP: false positive, FN: false negative. Red bounding boxes represent the detected artifact with top prediction scores, blue bounding boxes represent other detected bounding boxes with the same class label, and green bounding boxes represent the ground truth.



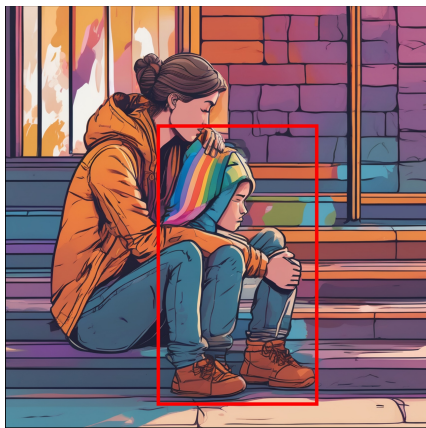
Figure 18. Examples of predictions from our HADM on unseen domains including SD1.4 (first row), PixArt- $\Sigma$  (second row), FLUX.1-dev (third row), and 300W (last row).



Negative As Positive

Original SDXL

Finetuned SDXL



Negative As Positive

Original SDXL

Finetuned SDXL

Figure 19. More results from the original SDXL model and our finetuned SDXL model. In the first column, images generated by the finetuned model use special identifiers as part of the prompt instead of as negative prompts. In the second and third columns, images from the original and the finetuned SDXL models use special identifiers as negative prompts.